Massimiliano Simi
The BioRobotics Institute,
Polo Sant'Anna Valdera,
Pisa 56025, Italy
Department of Mechanical Engineering,
Vanderbilt University,
Nashville, TN 37212
e-mail: m.simi@sssup.it

Giada Gerboni
e-mail: g.gerboni@sssup.it

Arianna Menciassi
e-mail: a.menciassi@sssup.it

The BioRobotics Institute,
Polo Sant'Anna Valdera,
Pisa 56025, Italy

Pietro Valdastri
Department of Mechanical Engineering,
Vanderbilt University,
Nashville, TN 37212
e-mail: p.valdastri@vanderbilt.edu

Magnetic Torsion Spring Mechanism for a Wireless Biopsy Capsule

The authors present a novel magnetomechanical elastic element that can be loaded remotely by varying the magnetic field surrounding it and that is able to store and release mechanical energy upon external triggering. The magnetic torsion spring (MTS) is used as the core component of a self-contained miniature biopsy capsule (9 mm in diameter and 24 mm long) for random tissue sampling in the small bowel. Thanks to the MTS concept, the biopsy mechanism can be loaded wirelessly by a magnetic field applied from outside the body of the patient. At the same time, magnetic coupling guarantees stabilization against the small bowel tissue during sampling. Extreme miniaturization is possible with the proposed approach since no electronics and no power supply are required onboard. [DOI: 10.1115/1.4025185]

1 Introduction

The small intestine is home to a number of increasingly common human diseases. Celiac disease alone has a worldwide prevalence of 1% (i.e., 70,000,000 patients) [1] and its incidence has been doubling every 15 years since 1974 [2]. Early diagnosis of small intestine diseases is crucial to enable effective therapy and prevent complications such as severe anemia or irreversible villous atrophy, especially in pediatric patients [3]. Unfortunately, the small intestine is the most difficult organ of the gastrointestinal (GI) tract to access due to its length (7 m in average) and distance from a natural body orifice [2]. Flexible endoscopy allows for reliable diagnosis—including collection of tissue samples under visual guidance—at the price of relevant patient discomfort and often requiring sedation [4]. Furthermore, this technique is not suitable for children younger than 3 yr due to its invasiveness [5].

Wireless capsule endoscopy (WCE) has emerged as a promising technique for diagnosis of suspected diseases in the small bowel since its introduction in 2001 [4]. Thanks to its low invasiveness, WCE is also a well-established diagnostic method for children [5], with the youngest child undergoing WCE reported so far being 8 months old [6]. Although in some cases visual information provided by WCE are sufficient for identifying GI lesions [7–9], this technique lacks the ability of collecting biopsy samples, which is crucial for an effective and definitive diagnosis [10]. In particular, random biopsies of small bowel tissue are required to diagnose celiac disease, malabsorption syndromes, food sensitivity, autoimmune disease, inflammatory small bowel disease, and small bowel infection [11].

The clinical need for a noninvasive technique to gather biopsy samples in the small intestine encouraged a relevant body of research in medical devices. The Crosby capsule, developed in 1957, was the first tethered device for GI tract biopsy collection [12]. Today, it is mainly used in children due to its small size (11 mm in diameter and 20 mm in length). Suction applied to the tube triggers an onboard mechanism that causes a spring-loaded knife to sweep across an aperture in the capsule, cutting away any mucosa protruding into the aperture and collecting the sample in a dedicated chamber. The presence of a tether—to assist with both biopsy collection and retrieval—and the need for X-ray to localize the capsule severely limited the impact of this device in terms of adoption. The first example of a wireless biopsy capsule consists of a rotational tissue-cutting razor attached to a torsion spring and constrained by a paraffin block [13]. When the paraffin block melts by heating, the razor is released, thus collecting a tissue sample. The biopsy module alone is 10 mm in diameter and 2 mm in thickness, but it requires additional space for control electronics and power supply. Another compact solution with the same size, designed to be integrated in the MiRo endoscopic capsule (Intro-Medic, Seoul, Korea), consists of a microbiopsy spike with protruding barbs, a spring, and a mechanism actuated by shape memory alloy (SMA) [14]. The device is designed to operate sequentially so that tissue sampling, sealing, and fixation are achieved in a single operation. However, it is not yet clear whether such a mechanism will be able to collect a sufficient number or volume of samples for accurate external histological analysis. In both of these solutions, system stabilization during tissue sampling remains as the main open issue (i.e., if the capsule is not anchored, the reaction force from the biopsy mechanism acting on the tissue may jeopardize tissue sampling effectiveness). This issue is addressed in Ref. [15], where a complete capsule device for tissue biopsy under visual guidance is proposed. This system is composed by a vision module, an anchoring module, and an SMA-based tissue sampling module. The three modules together were integrated into a 40 mm long by 15 mm in diameter capsule, which, however, does not include power supply. This highlights a significant limitation for all the proposed solutions, that is, the need for onboard control electronics and power supply. Given the tight volume constraint for a swallowable device, the design of a biopsy mechanism that relies an onboard power supply and wireless electronics for triggering and operation may not be a viable solution, particularly if the biopsy device is intended for pediatric patients.

Manuscript received October 2, 2012; final manuscript received July 16, 2013; published online September 24, 2013. Assoc. Editor: William K. Durfee.

In this paper, we introduce the novel concept of magnetic torsion spring (MTS) and we leverage it to design a self-contained miniature biopsy capsule for random tissue sampling in the small bowel. Thanks to the MTS concept, the biopsy mechanism can be loaded wirelessly by a magnetic field applied from outside the body of the patient. At the same time, magnetic coupling guarantees stabilization against the small bowel tissue during sampling. Extreme miniaturization is possible with the proposed approach since no electronics and no power supply are required onboard.

The remainder of this paper is organized as follows. The main design specifications are provided in Sec. 2. Section 3 describes the principle of operation for both the MTS and the wireless biopsy capsule. The capsule design is described in Sec. 4, while fabrication and assembly are detailed in Sec. 5. Experimental assessment is reported in Sec. 6, while Sec. 7 outlines conclusions and future directions.

2 Design Specifications

Design requirements to develop a miniature biopsy capsule for random tissue sampling in the small bowel are mainly determined by medical considerations and functionality constraints as follows.

Size. The smaller the volume of the capsule, the larger will be the population able to swallow it, possibly including children. Although "swallowable" is somewhat challenging to define—because the maximum swallowable size varies from person to person—we can reasonably target state-of-the-art WCE devices. In particular, Given Imaging PillCam SB2 [4]—which is 11 mm in diameter and 26 mm in length—has been approved by Food and Drug Administration in 2001 for use in adults and in 2003 for use in children older than 10 yr [5].

Tissue Sampling—Cutting Pressure. The biopsy mechanism must provide a sufficient force—or torque, depending on the mechanism design—to cut a tissue sample. An average value of 1 MPa at the tool–tissue interface is assumed as destructive stress for GI tract tissues, as reported for human cadaver trials [16].

Tissue Sampling—Stabilization. For an effective sampling, the capsule must firmly adhere to the tissue and balance the reaction force (or torque) while operating the biopsy mechanism.

Tissue Sampling—Storage. Typically, a small bowel biopsy test consists in one to five tissue samples approximately 1 mm^3 in volume [10,17–19]. Therefore, an ideal biopsy mechanism needs to collect and preserve multiple samples in a total storage volume larger than 5 mm^3. Cross-contamination of tissue samples in the same reservoir does not alter the diagnostic value for diffuse GI diseases, such as celiac disease. Concerning preservation, intestinal biopsy samples can be stored up to 24 h on a gauze soaked with liquid solution, still preserving their diagnostic significance [20].

Safety. The sampling mechanism design must be fail safe, possibly avoiding parts protruding from the surface of the capsule and the risk of lumen perforation.

Localization. Since we target random biopsies in the small intestine, the main purpose of localization for the proposed application is to detect when the capsule has reached the small intestine. Therefore, simultaneous localization and biopsy is not required. Localization methods based on ionizing radiation should be avoided for the sake of patient safety.

3 A Novel Biopsy Capsule Design Based on Magnetic Torsion Springs

The standard approach in designing active medical devices builds upon mechatronics. Most of the miniature active capsules for GI applications reported to date integrate sensors, actuators, programmable electronics, wireless communication, and power supply [21]. Miniaturizing all these components to fit a swallowable volume poses several challenges that severely limit the translational impact of novel designs.

The solution we propose relies completely on passive components and leverages magnetic fields to remotely operate a mechanism that satisfies the above-mentioned specifications.

3.1 Magnetic Torsion Spring—Principle of Operation.

The core component of our design is the magnetic torsion spring (MTS), a novel magnetomechanical elastic element that can be loaded remotely by varying the magnetic field surrounding it and that is able to store and release mechanical energy upon external triggering.

A single MTS, represented in Fig. 1, is composed by two coaxial cylindrical diametrically magnetized permanent magnets. One magnet is mounted on a shaft and is free to rotate, while the other one is constrained to the body of the device where the MTS is integrated.

Defining θ as the relative displacement angle between the two magnets, the magnet free to rotate will orient itself to zero under the effect of the local magnetic coupling. If an external magnetic field with opposite polarity of the MTS-constrained magnet and strong enough to overcome local interaction between the two MTS magnets is applied, θ will reach π, storing elastic potential energy into the mechanism. Then, the sudden removal of the external magnetic field will trigger the release of the magnetic spring, which will zero θ again under the effect of the local magnetic coupling between the two MTS magnets. During this transition, all the elastic energy stored in the MTS is transformed to kinetic energy that can be used by the mechanism to perform its specific task.

3.2 Magnetic Torsion Spring—Analytical Description.

Unlike a conventional torsion spring, the MTS has a nonlinear torque transfer function [22] that can be estimated as follows:

$$T_m(\theta) = T_p \cdot \sin\theta \tag{1}$$

where T_m represents the torque required to displace the magnet free to rotate of an angle θ from the $\theta = 0$ position, while T_p represents the peak torque, that is a function of MTS design (i.e., T_p depends on the distance between the two MTS magnets and on the geometry and magnetization of each MTS magnet). The analytical model described in Ref. [23] or finite element analysis software (e.g., COMSOL MultiPhysics, Sweden) can be used to quantify T_p by considering the MTS at $\theta = \pi/2$ (i.e., $T_m(\pi/2) = T_p$).

The elastic potential energy stored in the MTS can be expressed by calculating the work required to displace the rotating magnet of an angle θ from the $\theta = 0$ position

$$U(\theta) = -W(\theta) = -\int_0^\theta T_m(\varphi)d\varphi \tag{2}$$

By substituting Eq. (1) in Eq. (2), we have

$$U(\theta) = -T_p\int_0^\theta \sin\varphi\, d\varphi = T_p(1-\cos\theta) \tag{3}$$

where the result of the integration is expressed in rad.

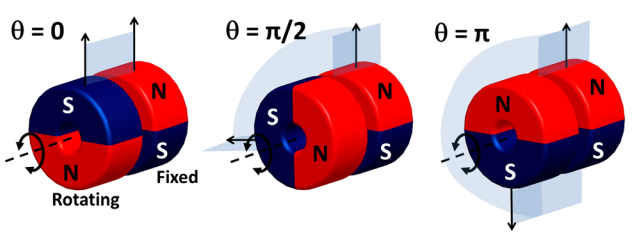

Fig. 1 The basic components of an MTS

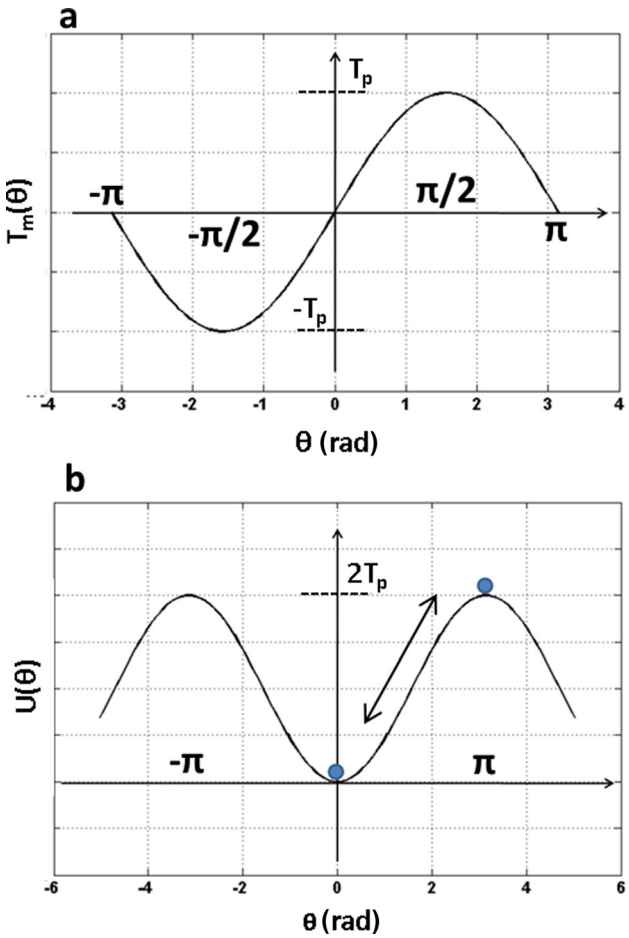

Fig. 2 (*a*) The MTS torque versus angular displacement of the rotating magnet. (*b*) The MTS potential energy as a function of the angular displacement of the rotating magnet.

Plots of $T_m(\theta)$ and $U(\theta)$ are represented in Figs. 2(*a*) and 2(*b*), respectively. The plot of the potential energy shows that the MTS possesses stable equilibrium points for $\theta = \pm n2\pi$, with $n = 0, 1, 2, 3\ldots$ and unstable equilibrium points for $\theta = \pi \pm n2\pi$, with $n = 0, 1, 2, 3\ldots$. In order to remotely load the MTS to its unstable equilibrium position, the external magnetic field must provide a torque larger than T_p at the MTS magnet that is free to rotate.

3.3 Wireless Biopsy Capsule—Principle of Operation. The proposed design for a wireless biopsy capsule is represented in Fig. 3 and takes advantage of two MTSs located at the two ends of the capsule. For each MTS, one cylindrical magnet is constrained to the body of the capsule, while the other one is mounted on a shaft together with a cylindrical razor blade. The external profile of the capsule has a lateral hole, which is closed by the blade for $\theta = 0$ (Fig. 3(*a*)), while is open to host tissue for $\theta = \pm\pi$ (Fig. 3(*b*)). Local coupling at the two MTSs maintains $\theta = 0$ in case no external magnetic field is present. In this configuration, the capsule can be swallowed by the patient. Transition from $\theta = 0$ to $\theta = \pm\pi$—thus opening the lateral hole and loading the MTSs—can be obtained by providing the appropriate external magnetic field as in Fig. 3(*b*), e.g., by placing a permanent magnet polarized outside the patient in the proximity of the biopsy capsule.

As represented in Fig. 4(*a*), the external magnetic field has also the function of attracting the biopsy capsule toward the lumen wall, thus promoting the superficial layer of the bowel to enter in the capsule lateral hole. By decreasing the intensity of the external magnetic field (e.g., by moving the external magnet away from

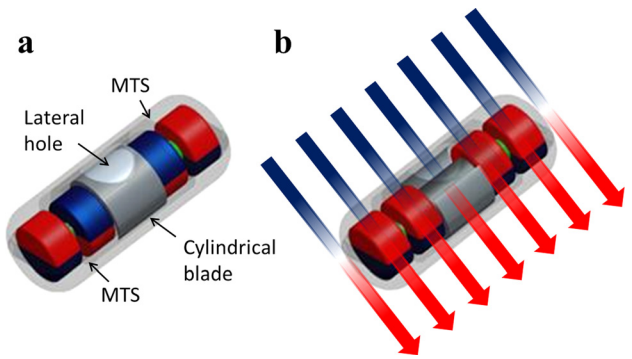

Fig. 3 (*a*) Wireless biopsy capsule design embedding two MTSs to actuate a cylindrical blade. (*b*) The application of an external magnetic field loads the MTSs and opens the lateral hole.

the patient), the MTSs-blade assembly moves back to its original position, thus cutting the tissue inside the hole and storing it within the capsule (Fig. 4(*b*)). Once the external magnetic field is completely removed, the capsule detaches from the lumen wall and is again free to move along the GI tract under the effect of peristalsis (Fig. 4(*c*)).

The proposed approach addresses all the design specifications discussed in Sec. 2. In particular, *size* is optimized by preventing the need for control electronics and onboard power supply. Adequate *cutting pressure* is provided by two MTSs—as better quantified in the rest of the paper. *Stabilization* is achieved by magnetic coupling between the capsule and the external permanent magnet. Reliable *storage* of the tissue sample is allowed by the cutting mechanism design. The absence of protruding parts enhances *safety*. As concerns localization, the permanent magnets inside the capsule allow for real-time position tracking with commercial platforms (e.g., 3D-Magma, Matesy GmbH, Germany). Magnetic localization—outside the scope of this paper—must be performed at a different time than biopsy since the external magnet will interfere with position tracking [24].

4 Design Flow

A stepwise approach has been adopted to address each design parameter in order to meet the specifications. The design flow started from the MTS permanent magnet selection and arrangement in order to maximize the available torque at the mechanism. Then, an external permanent magnet that was able to remotely load the mechanism and appropriately stabilize the capsule

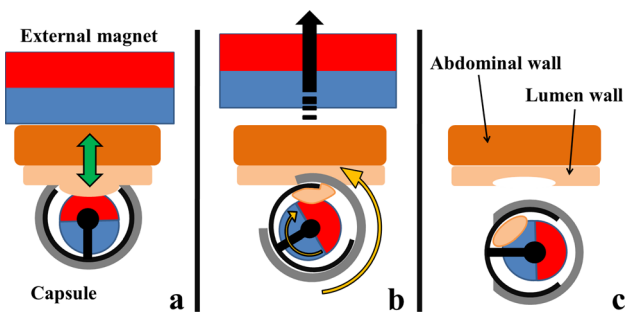

Fig. 4 Section view of the biopsy capsule operation principle. (*a*) Applying an external magnetic field the capsule is attracted toward the lumen wall, the lateral hole is open, and the MTSs are loaded. (*b*) Removing the external magnetic field triggers the MTSs and the blade rotation cuts and stores a tissue sample. (*c*) Without any external magnetic field, the biopsy capsule is closed and travels along the GI tract under the effect of peristalsis.

against the GI tissue was selected. The size of the lateral hole was defined by taking into account the attraction force between the external magnet and the capsule, while having in mind the desired sample volume. Finally, the blade geometrical features were selected considering the magnetic torque transmitted, the hole size, and the average pressure required to cut GI tissue.

4.1 MTS Design. The first step in the design flow consisted in selecting the permanent magnets for the MTS. Given the constraint in capsule diameter, we maximized the magnetic coupling by selecting permanent magnets with the strongest magnetization currently available for a doughnut-shaped magnet. Therefore, we selected off-the-shelf cylindrical diametrically-magnetized NdFeB permanent magnets, 6.3 mm in outer diameter, 1 mm in inner diameter, and 3.2 mm in thickness, with N52 magnetization (magnetic remanence of 1.48 T) (KJ Magnetics, Jamison, PA).

The second design choice was to fix the distance (d_m) between the two doughnut-shaped magnets of the MTS. As previously mentioned, the maximum torque that a MTS can release (T_p) depends on MTS magnet features and their relative distance (d_m). On the other hand, T_p is the torque that the external magnetic field must overcome in order to remotely load the MTS. In order to quantify T_p as a function of d_m, finite element analysis software (COMSOL MultiPhysics, Sweden) was used and the results are represented in Fig. 5. In particular T_p was calculated fixing $\theta = \pi/2$ and for d_m increasing in 0.25 mm steps from 0.5 mm to 3 mm neglecting any friction effect.

A value of $d = 1$ mm, thus $T_p = 5.3$ mNm, was selected as trade-off between MTS maximum torque and remote loading ability. However, if multiple MTSs are spaced far enough not to interact each other, the same magnetic field required to open a single MTS shall open all of them. This can be easily demonstrated by considering the superposition of effects, which holds true for magnetic fields when no other ferromagnetic materials are present in the environment. Therefore, we decided to use two MTSs mounted on the same shaft to double the total torque available at the tissue-cutting mechanism, without increasing the requirements in terms of external magnetic field. To prevent cross coupling, the two MTSs were spaced as much as the design constraint on capsule length allowed, i.e., $d_s = 7$ mm, and a finite element simulation was performed to confirm the absence of magnetic interaction. It is also worth mentioning that using two MTSs increases the attraction force toward the external permanent magnet, potentially improving anchoring while tissue is being cut. Furthermore, if the cutting mechanism is placed in between the two MTSs as in Fig. 3, design symmetry guarantees a uniform pressure of the sampling cavity onto the tissue.

Given this configuration (two MTSs with $d_m = 1$ mm separated by $d_s = 7$ mm), a dedicated finite element simulation was performed to obtain $T_{m2}(\theta)$—where subscript 2 is used for quantities related to two MTSs—for θ ranging from 0 to π. The angular displacement π was increased in steps of 0.0175 rad (equal to 1 deg) from 0 to π. A screenshot from the simulation for $\theta = 0$ is represented in Fig. 6(*a*).

In order to validate the simulation results and to experimentally quantify $T_{m2}(\theta)$ in the same range of θ, a dedicated bench test was set up. Two MTSs—spaced 7 mm apart—were embedded into a plastic chassis. The two magnets free to rotate were connected to a spool (diameter $b = 14$ mm) connected to a load cell (Nano 17-E, ATI Industrial Automation, U.S.) through an inextensible Dacron string, as sketched in Fig. 6(*b*). The load cell was mounted on a linear slider. Force was recorded while the slider was pulling the load cell away from the spool with a speed of 0.1 mm/s (i.e., quasi-static conditions). The range of motion of the slider was selected so to vary θ from 0 to π. This trial was repeated ten times and the results were averaged.

Simulated and experimental trends for $T_{m2}(\theta)$ are reported in Fig. 7. Average root mean square error when comparing simulated to experimental data was 0.618 mNm. The simulated value for the total maximum torque T_{p2} available at the mechanism is 10.7 mNm. This value is almost two times T_p, thus confirming that no significant magnetic interaction was occurring between the two MTSs. The experimental value for T_{p2} is 11 mNm. The 0.3 mNm deviation from the simulation results can be explained by considering the dynamic friction of the spool.

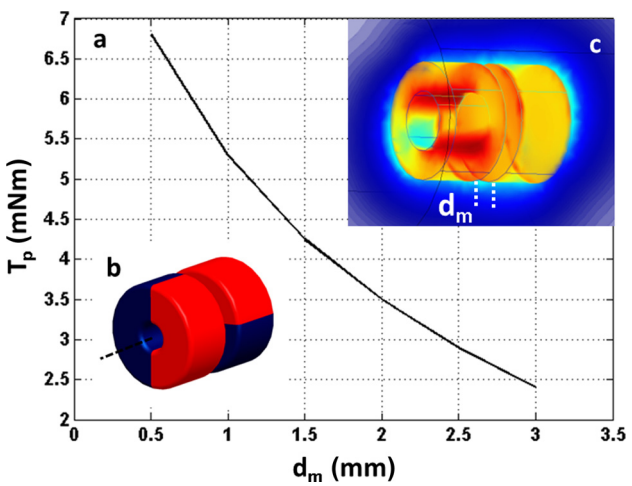

Fig. 5 (*a*) The MTS maximum magnetic torque ($\theta = \pm\pi/2$) as a function of MTS magnet distance obtained by finite element simulation. Scheme of the (*b*) magnetic configuration and (*c*) simulation screenshot. Magnet properties, such as shape, dimension, magnetization direction, remanence, and magnetic permeability ($\mu_0 = 1.05$) were set into the simulation. The selected mesh consisted of approximately 150,000 elements with a maximum element size set at 1/50 of the maximum geometric feature in the scenario.

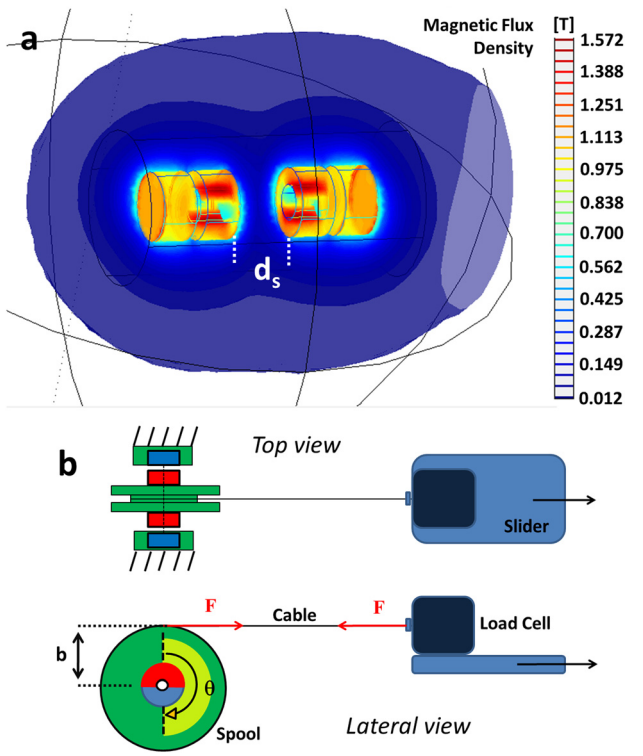

Fig. 6 (*a*) Screenshot for the finite element simulation for $\theta = 0$. The selected mesh consisted of approximately 250,000 elements with a maximum element size set at 1/50 of the maximum geometric feature in the scenario. (*b*) Sketch of the experimental bench test used to assess $T_{m2}(\theta)$.

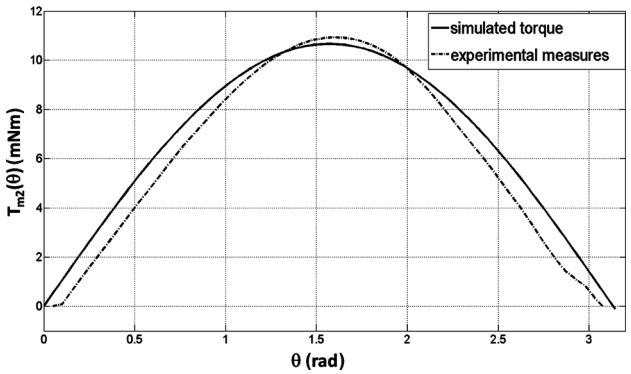

Fig. 7 Simulated and experimental trends for $T_{m2}(\theta)$

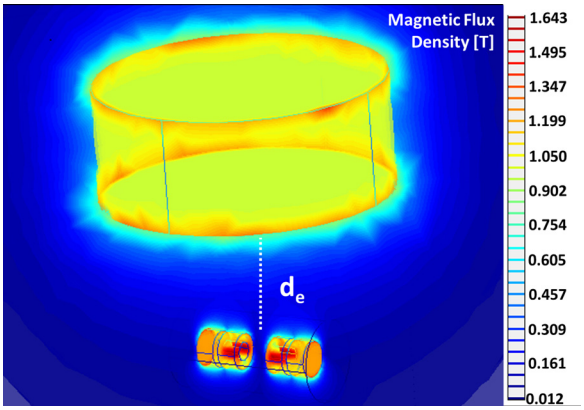

Fig. 8 Finite element simulation screenshot for estimating the torque exerted by the external permanent magnet on two MTSs located $d_e = 27$ mm away on the vertical axis. The two MTSs were spaced $d_s = 7$ mm each other and $\theta = 0$ was assumed. The mesh consisted of approximately 380,000 elements with a maximum element size set at 1/50 of the maximum geometric feature in the scenario.

4.2 External Magnetic Field Generation. The external magnetic field has the dual function of loading the MTSs to their unstable equilibrium condition and attracting the biopsy capsule towards the small intestine wall.

A single MTS can be loaded if the external magnetic field is able to generate at least a torque of 5.3 mNm at the MTS magnet free to rotate. This corresponds to a magnetic flux density of 103.5 mT, as results from an additional purposely developed finite element simulation. As previously mentioned, if multiple MTSs are spaced enough not to interact each other, the same magnetic field required to open a single MTS shall open all of them. Therefore, the magnetic field source must be able to generate a uniform magnetic flux larger than 103.5 mT at the capsule from a distance outside the body of the patient. This value is far below the safety threshold of 2 T recommended for occupational exposure in Ref. [25]. The magnetic field also needs a gradient along the its main direction to guarantee a stable anchoring of the capsule against the intestine wall.

While there are precise constraints on the external magnetic field value, there are no stringent requirements for the size of the field generator since it is located outside the patient's body. Electromagnetic field generators [26,27] are the best option to obtain a uniform magnetic field that can be controlled in intensity and gradient. We decided to use an off-the-shelf permanent magnet to prove the principle with the simplest and cheapest possible approach. This is particularly relevant for a potential translation of a novel medical device since deployment costs are always one of the main barriers to adoption. We selected a disk-shaped NdFeB permanent magnet (50 mm in diameter and 20 mm in thickness) with an N52 axial magnetization (Fig. 8). A finite element simulation was performed to evaluate the distance from the disk-shaped magnet where the magnetic flux density is large enough to load the MTS, the uniformity of the flux density in that region, and the gradient of the field. Then, a second finite element simulation was performed by adding to the previous scenario the second MTS (features as detailed in Sec. 4.1) in the region where the magnetic flux density is large enough to load them. The aim of this second set of simulations was to estimate the torque induced by the external magnet on the two MTSs for $\theta = 0$ to confirm that it corresponds to T_{p2}, thus strong enough to fully load the MTSs. Finally, a third simulation was performed varying the distance between the disk-shaped magnet and the two MTSs while keeping the two boundary conditions—i.e., mechanism closed $\theta = 0$ and mechanism open $\theta = \pi$—to quantify the trend of the attraction force. For this simulation, the distance between the disk-shaped magnet and the two MTSs was varied from 10.5 mm down to 0.5 mm in steps of 0.5 mm. This range is typically used for magnetic locomotion of capsule endoscopes [4,28] and is valid for a population with a body mass index (BMI) up to 30.

In order to assess the simulation results and to obtain the experimental trend of the attraction force within the two boundary conditions, which corresponds to the attraction force effectively available during cutting, while the mechanism goes from open to close, we set up the bench test sketched in Fig. 9. In particular, two MTSs were spaced 7 mm apart inside a plastic capsule (9 mm in diameter and 24 mm in length) and the two magnets free to rotate were glued on a plastic shaft mounted on synthetic ruby bushes. The capsule was connected to the load cell through an inextensible cable and the magnetic attraction force was acquired while incrementally positioning the load cell-capsule assembly toward the disk-shaped permanent magnet with a slider. This setup allows for a quantification of the magnetic attraction force with the MTSs free to rotate under the action of the external magnetic field.

Concerning simulation results, the selected disk-shaped magnet was able to provide a magnetic flux density of 103.5 mT at 27 mm from its circular surface, thus generating a torque at the two MTSs for $\theta = 0$ of 10.7 mNm (a screenshot of this simulation is represented in Fig. 8). Assuming a two-MTS capsule with its center 27 mm away from the disk-shaped magnet, the variation of magnetic flux density at the two MTSs is below 1%, while the gradient along the direction connecting the center of the external magnet and the center of the capsule is − 7.5 T/m. Attraction force along the same direction is plotted in Fig. 10 as a result from simulations and from experimental data. The experimental plot overlays the simulated trend except for the distance range related to the transition from $\theta = \pi$ to $\theta = 0$, occurring for a magnet-capsule distance (d_e) ranging from 27 mm to 50 mm.

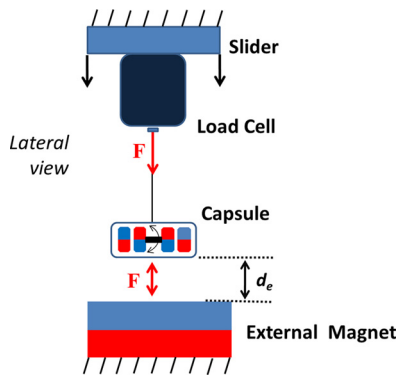

Fig. 9 Sketch of the experimental setup to measure the magnetic attraction force between a capsule embedding two MTSs and the chosen external permanent magnet

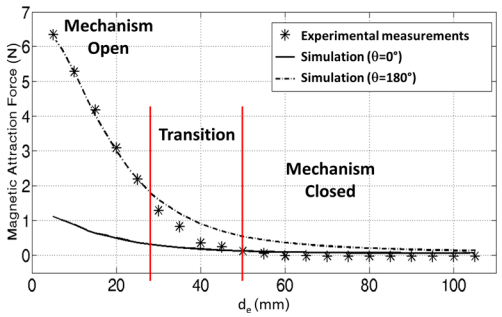

Fig. 10 Plot of the magnetic attraction force between the external permanent magnet and the biopsy capsule embedding two MTSs as a function of d_e. Simulation results for $\theta = 0$ and $\theta = \pi$ superimposed to experimental data.

Furthermore, the magnetic attraction force is at least 2 N when the mechanism is open. We expect this force promotes the superficial layer of the bowel to enter in the capsule lateral hole. During the transition from open to closed condition, this force drops down to 0.18 N (value of the magnetic attraction force at a magnet-capsule distance of 50 mm), while the MTSs release their elastic potential energy and the blade closes the hole completely, thus cutting the tissue. This range of values for the attraction force has to be taken into account when designing the diameter of the later cavity and the blade shape in order to achieve the desired sample volume of 1 mm^3.

4.3 Hole Dimensioning. Once characterized the trend of the force attracting the capsule to the intestinal wall (Fig. 10), we focused on selecting the diameter of the lateral hole that would guarantee the penetration of at least 1 mm^3 of tissue (typically 1 mm thick). Five capsule mock-ups (9 mm in diameter) with lateral hole diameters ranging from 3 mm to 7 mm in steps of 1 mm were fabricated by rapid prototyping. This range is centered on 5 mm, which is the diameter of the hole for the Crosby capsule [12]. Each capsule mock-up was connected to a load cell mounted on a vertical slider and pressed against the inside of a freshly excised porcine small intestine sample. The tissue sample was fixed to a layer of artificial skin to mimic the compliance of abdominal organs. A high-definition camera was mounted on the side of the experimental setup to quantify the height of the tissue penetrating the hole. Image analysis software ImageJ v1.46 was used on each acquired image to extract the numeric values for the tissue height. For each capsule mock-up, penetration depths were acquired for two different values of compression force, i.e., the maximum (2 N) and the minimum (0.18 N) of the magnetic attraction force.

An approximation of the volume of the tissue inside the lateral hole as a spherical cap can be expressed as

$$V = \frac{\pi h}{6}\left(\frac{3}{4}(d/2)^2 + h^2\right) \tag{4}$$

where d is the diameter of the hole and h is the measured penetration height. Each measurement was repeated for five times and the results were averaged. A sketch of the setup is reported in Fig. 11.

Given the experimental results, reported in Table 1, a lateral hole of 4 mm in diameter is not able to guarantee enough tissue penetration to collect a tissue sample larger than 1 mm^3 for the entire attraction force range. On the other hand, a lateral hole of 6 mm in diameter—or larger—may jeopardize safety by allowing the full thickness of the small intestine to enter into the cavity. Therefore, to meet the requirements in terms of tissue sample volume and to prevent small intestine perforation at the time of tissue cutting, a lateral hole of 5 mm in diameter was adopted for the proposed design.

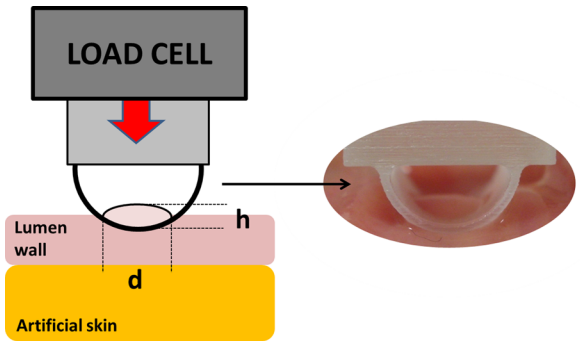

Fig. 11 (*a*) Sketch of the experimental setup to estimate the typical volume of the tissue penetrating the lateral hole as a function of the hole diameter. Image of a capsule mock-up, with a 5 mm hole, pressed against an excised porcine small intestine sample.

Table 1 Tissue volume penetrating inside the hole for different hole diameters and compression force

Mock-up diameter	Tissue volume for 2 N of compression force	Tissue volume for 0.18 N of compression force
3 mm	0.3 mm^3 (σ_x: 35×10^{-2})	0.0 mm^3 (σ_x: 13×10^{-2})
4 mm	1.3 mm^3 (σ_x: 31×10^{-2})	0.7 mm^3 (σ_x: 36×10^{-2})
5 mm	4.3 mm^3 (σ_x: 33×10^{-2})	1.5 mm^3 (σ_x: 35×10^{-2})
6 mm	8.5 mm^3 (σ_x: 30×10^{-2})	4 mm^3 (σ_x: 33×10^{-2})
7 mm	13.8 mm^3 (σ_x: 25×10^{-2})	7.4 mm^3 (σ_x: 29×10^{-2})

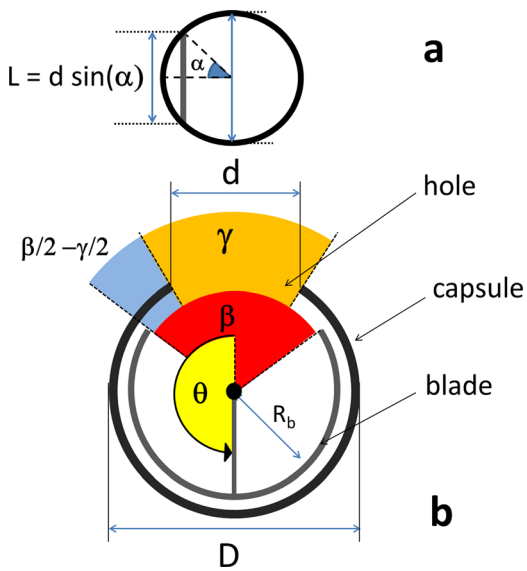

Fig. 12 Top view of (*a*) the lateral hole and (*b*) central cross section of the biopsy capsule

4.4 Blade Design. In order to motivate the choices made for the dimensioning of the blade, an analytical description of the pressure that it exerts on the tissue as a function of θ is provided for θ ranging from $\pm\pi$ to 0. This formulation is then used to verify that the pressure exceeds the average destructive stress for GI tissues of 1 MPa [16] for the entire range of motion of the blade.

Referring to Fig. 12(*b*), we define the following parameters:

- R_b as the cylindrical blade outer radius. In order to obtain the largest possible lever for T_{m2}, this value must be minimized as much as fabrication and assembly constraints allow.

On the other hand, this parameter must be close to the inner diameter of the capsule to guarantee an effective grip of the blade on the tissue penetrating the lateral hole. Since the inner diameter of the capsule body is 7.2 mm, we chose $R_b = 3.55$ mm to leave enough room for blade rotation. With this selection, a maximum force of 3.1 N can be applied to the tissue.

- t as the thickness of the blade. This parameter must be minimized in order to increase the cutting pressure. It strictly depends upon the fabrication technology adopted for the blade. As better detailed in the following subsection, the blade was fabricated by micro-electro-discharge-machining (μEDM). This technology allowed for $t = 30\,\mu$m. This same thickness was adopted in Ref. [15] for the same application.
- γ as the capsule lateral hole angular opening. This quantity is two times the arcsine of the ratio between the hole radius ($d/2$) and the capsule radius ($D/2$). From the previous steps of the design flow, we can assume $d = 5$ mm and $D = 9$ mm, thus resulting in $\gamma = 1.178$ rad (67.5 deg).
- β as the blade angular opening. This is the main free design parameter for the blade and it affects the range of θ where the blade starts to cut the tissue, as better detailed below.

Since $\theta = \pm\pi$ is an unstable equilibrium condition—thus the blade can rotate either clockwise ($d\theta/dt > 0$) or counterclockwise ($d\theta/dt < 0$) when the mechanism is triggered—the blade must approach the tissue in the same way disregarding the direction of rotation. Therefore, symmetry constraints apply to the blade shape. In particular, the center of the blade opening for $\theta = \pm\pi$ must coincide to the center of the lateral hole in the capsule and the blade must be symmetric along the vertical axis of Fig. 12(*b*).

To better underline the role of β, it is possible to define the angles $\pm\theta_1$ and $\pm\theta_2$ where the blade starts and ends to cut the tissue, respectively. While the sign depends on the direction of rotation of the blade, the absolute values can be expressed as follows:

$$\theta_1 = \pi - \left(\frac{\beta}{2} - \frac{\gamma}{2}\right) \tag{5}$$

$$\theta_2 = \pi - \left(\frac{\beta}{2} + \frac{\gamma}{2}\right) \tag{6}$$

The pressure exerted by the blade on the tissue as a function of θ can then be expressed as

$$P(\theta) = \frac{((T_{p2}\sin\theta)/R_b)}{S(\theta)} \quad \text{for} \quad \theta_2 < |\theta| < \theta_1 \tag{7a}$$

where $S(\theta)$ is blade surface in contact with the tissue as a function of θ. Referring to Fig. 12(*a*), $S(\theta)$ can be seen as the product of t and $L(\theta)$, defined as the lateral dimension of the blade that overlaps the lateral opening for a given θ. This quantity can be expressed as

$$L(\theta) = d\sin(\alpha) \tag{7b}$$

where

$$\alpha = \pi\frac{\theta - \theta_1}{\gamma} \tag{7c}$$

By substituting Eq. (7*c*) in Eq. (7*b*) and then in Eq. (7*a*), we have

$$P(\theta) = \frac{((T_{p2}\sin\theta)/R_b)}{t \cdot d\sin[\pi \cdot (\theta - \theta_1)/\gamma]} \quad \text{for} \quad \theta_2 < |\theta| < \theta_1 \tag{8}$$

In order to start cutting the tissue when the attraction force—thus the stabilization against the tissue—is maximum, we decided to fix β so as to have $\theta_1 = \pi$, thus $\beta = \gamma = 67.5$ deg and $\theta_2 = 112.5$ deg. The value of $P(\theta)$ for θ ranging from θ_1 to θ_2 is represented in Fig. 13 and it is always larger than 1 MPa. It is worth mentioning that, with the current design choices, the mechanism ends the cut before reaching the peak of torque (T_{p2}, that is achieved for $\theta = \pi/2$). This is mainly due to the selection of the lateral hole diameter, that directly affects γ.

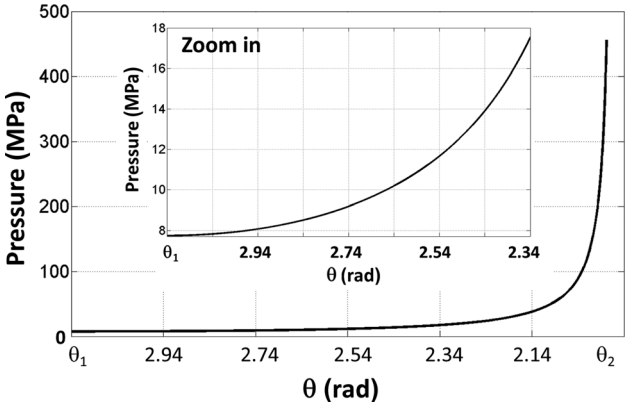

Fig. 13 Plot of the theoretical pressure exerted by the blade on the tissue during cutting for the selected design parameters

5 Capsule Fabrication and Assembly

Once all the main design parameters were fixed, each component of the capsule was either purchased or fabricated. Since the focus of this work was to prove the feasibility of the proposed approach, we did not focus on biocompatibility at this stage. Nevertheless, we see no relevant issues other than selection of materials, costs, and sterile environment assembly that would prevent full biocompatibility for GI applications.

All the permanent magnets were purchased off-the-shelf from the same supplier (KJ Magnetics, Jamison, PA)

The shaft and the cylindrical blade were fabricated in Ergal™ (i.e., 7075 aluminum alloy) in order to guarantee high stiffness to avoid magnetic interaction with the MTSs.

As represented in Figs. 14(*a*) and 14(*b*), the shaft is 15 mm long and has three different diameters. The central part is 4 mm in diameter and hosts a T-shape groove in the profile to mate with the cylindrical blade (Fig. 14(*d*)). The intermediate parts are 1 mm in diameter to fit in the central hole of the MTSs rotating magnets. The lateral parts of the shaft have a diameter of 0.8 mm to enable the connection with custom-made bushes in synthetic ruby (2.3 mm outer diameter and 0.8 mm in thickness, having a buffing surface to minimize friction) (Fig. 14(*e*)). A five-axis microcomputer numerical control (μCNC) center (HSPC, KERN GmbH, Germany) was used to fabricate the shaft.

Starting from the 7.1 mm in diameter and 7 mm long Ergal™ cylinder, the blade was machined as shown in Fig. 14(*c*) by μEDM (AP 200L, Sodick, Japan) and then fitted into the T-shape groove obtained in the shaft. The lateral profile of the blade guarantees a volume of 40 mm^3 as reservoir for tissue samples. This volume is larger than the 5 mm^3 that would be required to host five 1 mm^3 samples.

The capsule chassis is composed by two complementary shells fabricated in plastic by stereolithographic rapid prototyping (3-D Printer Invision Si2, 3D Systems Inc., U.S.) (Fig. 14(*g*)). The two MTSs rotating magnets were glued (Loctite 401) to the shaft so that their magnetization directions are parallel. Similarly, the two MTSs fixed magnets were glued to the chassis so that their magnetization directions are parallel. The assembly of the shaft, the blade, the rotating magnets, and the ruby bushes was mounted at the center of the capsule.

In order to provide a sharp edge to the hole, thus promoting tissue cutting, a metallic layer was aligned with the chassis lateral

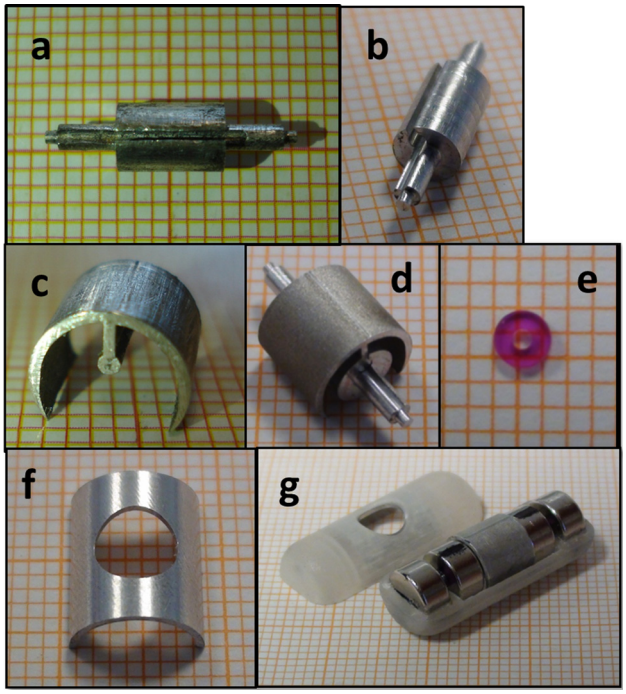

Fig. 14 Capsule components: (*a, b*) the shaft and (*c*) the blade (*d*) assembled together. (*e*) The ruby bushings and (*f*) the metallic layer assembled in (*g*) the prototype.

hole and glued on the inner side of the shell. This metallic part—represented in Fig. 14(*f*)—was fabricated in Ergal™ with a thickness of 0.5 mm, a length of 6 mm, a width of 5 mm, and outer and inner diameter of 8.10 mm and 7.10 mm, respectively, and with a 5 mm central hole.

Once all the components were embedded in the chassis, the two plastic shells were mated and glued together, obtaining a working prototype of the capsule that is 9 mm in diameter and 24 mm in length, with a 5 mm lateral hole along its profile (Fig. 15). The weight of the capsule prototype is 4.2 g.

6 Experimental Assessment

A single test was performed on the capsule prototype before assessing tissue sampling through dedicated ex vivo trials

The goal of the bench test was to assess the correct opening of the lateral hole of the capsule—thus the loading of the MTSs—with the external permanent magnet 27 mm away. The capsule was fixed to the bench, exposing the lateral hole on the top side. The external magnet was mounted on a vertical slider and made to approach the capsule ten times. For each trial, the complete opening of the lateral hole was observed when the external magnet was 27 mm away from the capsule, as expected.

Fig. 15 Assembled biopsy capsule prototype laying on graph paper for reference

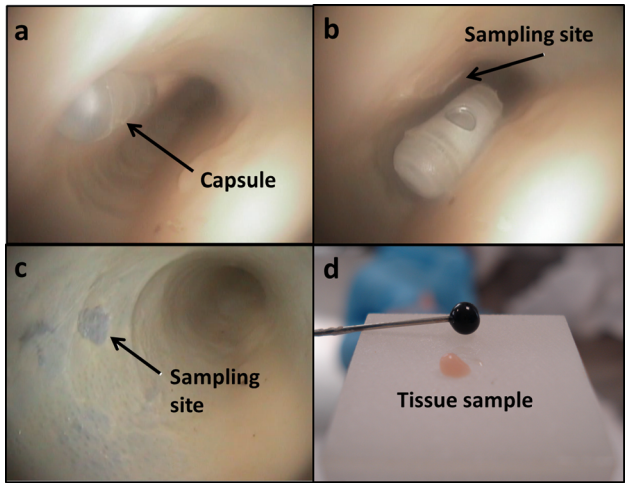

Fig. 16 Ex vivo trials. (*a*) The capsule is lifted against the tissue by magnetic interaction with the external magnet, while the MTSs are loaded. (*b*) Removing the external magnet the MTSs turn the blade, cutting a sample. (*c*) The lumen wall region where the sample has been removed. (*d*) The biopsy sample retrieved from the capsule.

Ex vivo trials were performed by using freshly excised porcine intestine segments, placed on an artificial skin layer, and covered with half-liter plastic bags filled with water to simulate the organs surrounding the lumen. Each segment was 30 cm long and was replaced after 15 min of use to minimize the effect of tissue degradation. Three different sessions of ex vivo trials were performed. The first aimed to observe the capsule behavior during the mechanism actuation. Therefore, the capsule was introduced into the lumen followed by a pediatric gastroscope (Karl Storz Endoscopy, Tuttlingen, Germany). The external magnet was manually moved on the outside of the lumen by an operator—at approximately 3 cm of distance—until magnetic coupling with the capsule was observed through the gastroscope (Fig. 16(*a*)). Then, the external magnet was moved out from the experimental setup and the capsule detached from the lumen, closing the mechanism, and cutting a layer of tissue (Figs. 16(*b*) and 16(*c*)). The capsule was then taken out from the lumen, the lateral hole was opened by placing the capsule close to the external magnet, and the tissue sample was retrieved using surgical tweezers. A typical tissue sample is represented in Fig. 16(*d*). This procedure—repeated ten times—provided the opportunity to familiarize the operator with the tissue sampling process.

The second session focused on blind operation of the biopsy capsule; therefore, the gastroscope was not used. The capsule was introduced randomly inside the lumen. The sampling mechanism was activated by slowly moving the external handheld magnet along the outside of the lumen, leveraging the experience gained during the previous session. The capsule was then removed from the lumen, the tissue sample was retrieved, and its volume was derived by measuring its weight. This procedure was repeated 20 times to achieve statistical relevance. The biopsy capsule was able to gather a tissue sample larger than 1 mm^3 all the 20 times. The lumen wall was never perforated by the blade and the mechanism never got stuck while cutting.

The third ex vivo session focused on multiple biopsy sampling. The same procedure of the previous session was followed moving the external magnet three times along the outside of the lumen, thus activating the mechanism for three times each trial. A total of five trials were performed and in all the cases the capsule was able to cut and safely store three different samples, each larger than 1 mm^3. However, it is worth mentioning that tissue degradation of the ex vivo intestinal tissue may favor tissue cutting. This effect is

not present in vivo, where tissue is continuously perfused. Therefore, an ultimate assessment of the proposed technology must be performed in vivo. This is outside the scope of this paper and will be the subject of future studies.

7 Conclusions and Future Directions

In this paper, a novel magnetomechanical elastic element—the MTS—was introduced, analyzed, and used as a remotely triggered actuator in a miniature wireless capsule for random biopsy in the small intestine. This approach allowed for extreme miniaturization (i.e., the capsule prototype was 9 mm in diameter and 24 mm in length) since no batteries and no control electronics were required on board. Remote loading of the cutting mechanism—obtained by an external permanent magnet—provided stabilization, anchoring, and a sufficient torque to acquire intestinal biopsies. Storage of multiple samples larger than 1 mm^3 was possible thanks to a large reservoir underneath the cylindrical rotating blade. The absence of parts protruding from the capsule profile guaranteed safety. The capsule position can be easily localized before biopsy by using commercial magnetic trackers [29], thanks to the onboard magnets.

The detailed description of the sequential design flow provided in this paper should pave the way for design variations. A different magnetic field source or a larger permanent magnet can be used to adapt the platform to patients with different BMI—thus requiring the capsule to be operated from a larger distance than 27 mm. To reduce the size of the capsule further, a single MTS can be used to operate the blade, provided that the pressure on the tissue is enough to cut.

Since the lack of miniature and efficient actuators is commonly identified as one of the main barriers to the design of capsule-size robots [4], the MTS has the potential to be an enabling component for a new generation of remotely controllable medical devices.

Further future directions for this work include extensive in vivo trials, the use of a soft sponge soaked in a weakly saline solution—to be included in the reservoir in order to promote biopsy preservation—and the study of a miniature sensing system to remotely detect the open and closed state of the mechanism.

Acknowledgment

The authors would like to thank N. Funaro and the staff of the BioRobotics Institute mechanical workshop for prototype manufacturing and Dr. Keith Obstein and Dr. Nicola Di Lorenzo for their medical suggestions. This work was supported in part by the ARAKNES European Project EU/IST-2008-224565 and by the National Center for Research Resources, Grant UL1 RR024975-01, and is now at the National Center for Advancing Translational Sciences, Grant 2 UL1 TR000445-06.

References

[1] Mubarak, A., Houwen, R. H., and Wolters, V. M., 2012, "Celiac Disease: An Overview From Pathophysiology to Treatment," Minerva Ped., **64**(3), pp. 271–287.
[2] Catassi, C., Kryszak, D., Bhatti, B., Sturgeon, C., Helzlsouer, K., Clipp, S. L., Gelfond, D., Puppa, E., Sferruzza, A., and Fasano, A., 2010, "Natural History of Celiac Disease Autoimmunity in a USA Cohort Followed Since 1974," Ann. Med. **42**(7), pp. 530–538.
[3] Tosco, A., Salvati, V., Auricchio, R., Maglio, M., Borrelli, M., Coruzzo, A., Paparo, F., Boffardi, M., Esposito, A., and D'Adamo, G., 2011, "Natural History of Potential Celiac Disease in Children," Clin. Gastroenterol. Hepatol., **9**(4), pp. 320–325.
[4] Valdastri, P., Simi, M., and Webster, R. J. III, 2010, "Advanced Technologies for Gastrointestinal Endoscopy," Ann. Rev. Biomed. Eng., **14**, pp. 397–429.
[5] de Ridder, L., Tabbers, M. M., and Escher, J. C., 2012, "Small Bowel Endoscopy in Children," Best Pract. Res. Clin. Gastroenterol., **26**, pp. 337–345.
[6] Nuutinen, H., Kolho, K. L., Salminen, P., Rintala, R., Koskenpato, J., Koivusalo, A., Sipponen, T., and Färkkilä, M., 2011, "Capsule Endoscopy in Pediatric Patients: Technique and Results in Our First 100 Consecutive Children," Scand. J. Gastroenterol., **46**(9), pp. 1138–1143.
[7] Spada, C., Riccioni, M., Urgesi, R., and Costamagna, G., 2008, "Capsule Endoscopy in Celiac Disease," World J. Gastroenterol., **14**(26), pp. 41–46.
[8] Rokkas, T. T., and Yaron, Y. N., 2012, "The Role of Video Capsule Endoscopy in the Diagnosis of Celiac Disease: A Meta-Analysis," Eur. J. Gastroenterol. Hepatol., **24**(3), pp. 303–308.
[9] Ersoy, O., Akin, E., Ugras, S., Buyukasik, S., Selvi, E., and Guney, G., 2009, "Capsule Endoscopy Findings in Celiac Disease," Digest. Disease. Sci., **54**(4), pp. 825–829.
[10] Catassi, C., and Fasano, A., 2010, "Celiac Disease Diagnosis: Simple Rules are Better Than Complicated Algorithms," Am. J. Med., **123**(8), pp. 691–693.
[11] Ludvigsson, J., Brandt, L., Montgomery, S., Granath, F., and Ekbom, A., 2009, "Validation Study of Villous Atrophy and Small Intestinal Inflammation in Swedish Biopsy Registers," BMC Gastroenterol., **9**(1), p. 19–22.
[12] Crosby, W. H., and Kugler, H. W., 1957, "Intraluminal Biopsy of the Small Intestine," Dig. Dis. Sci., **2**(5), pp. 236–241.
[13] Kong, K., Cha, J., Jeon, D., and Cho, D. D., 2005, "A Rotational Micro Biopsy Device for the Capsule Endoscope," Proc. IEEE/RSJ International Conference on Intelligent Robots and Systems (IROS 2005), Edmonton, Canada, August 2–6, pp. 1839–1843.
[14] Park, S., Koo, K., Bang, S. M., Park, J. Y., Song, S. Y., and Cho, D. D., 2008, "A Novel Microactuator for Microbiopsy in Capsular Endoscopes," J. Micromech. Microeng., **18**, pp. 25–32.
[15] Kong, K., Yim, S., Choi, S., and Jeon, D., 2012, "A Robotic Biopsy Device for Capsule Endoscopy," ASME J. Med. Device., **6**, pp. 31–40.
[16] Egorov, V., Schastlivtsev, I., Prut, E., Baranov, A., and Turusov, R., 2002, "Mechanical Properties of the Human Gastrointestinal Tract," J. Biomech., **35**(10), pp. 1417–1425.
[17] Hopper, A., Cross, S., Sanders, D., and Patchy, D., 2008, "Villous Atrophy in Adult Patients With Suspected Gluten-Sensitive Enteropathy: Is a Multiple Duodenal Biopsy Strategy Appropriate?," Endoscopy, **40**(3), pp. 219–224.
[18] Pais, W., Duerksen, D., Pettigrew, N., and Bernstein, C., 2008, "How Many Duodenal Biopsy Specimens are Required to Make a Diagnosis of Celiac Disease?," Gastrointest. Endosc., **67**(7), pp. 1082–1087.
[19] Dewar, D., and Ciclitira, P., 2005, "Clinical Features and Diagnosis of Celiac Disease," Gastroenterology, **128**(4), pp. 19–24.
[20] Browning, T., and Trier, J., 1963, "Organ Culture of Mucosal Biopsies of Human Small Intestine," J. Clinical Invest., **48**(8), pp. 1423–1432.
[21] Toennies, J. L., Tortora, G., Simi, M., Valdastri, P., and Webster, R. J. III, 2010, "Swallowable Medical Devices for Diagnosis and Surgery: The State of the Art," Proc. IMechE C: J. Mech. Eng. Sci., **224**(C7), pp. 1397–1414.
[22] Montague, R., Bingham, C., and Atallah, K., 2011, "Servo Control of Magnetic Gears," IEEE/ASME Trans. Mechatron., **17**(2), pp. 269–278.
[23] Di Natali, C., Ranzani, T., Simi, M., Menciassi, A., and Valdastri, P., 2012, "Trans-Abdominal Active Magnetic Linkage for Robotic Surgery: Concept Definition and Model Assessment," Proc. of IEEE International Conference on Robotics and Automation (ICRA) 2012, St Paul, MN, May 14–18, pp. 695–700.
[24] Salerno, M., Ciuti, G., Lucarini, G., Rizzo, R., Valdastri, P., Menciassi, A., Landi, A., and Dario, P., 2012, "A Discrete Time Localization Method for Capsule Endoscopy Based on On-Board Magnetic Sensing," Meas. Sci. Technol., **23**, p. 015701.
[25] International Commission on Non-Ionizing Radiation Protection (ICNIRP), 2009, "Guidelines on Limits of Exposure to Static Magnetic Fields," Health Phys., **96**(4), pp. 504–514.
[26] Rey, J. F., Ogata, H., Hosoe, N., Ohtsuka, K., Ogata, N., Ikeda, K., Aihara, H., Pangtay, I., Hibi, T., Kudo, S. E., and Tajiri, H., 2012, "Blinded Nonrandomized Comparative Study of Gastric Examination With a Magnetically Guided Capsule Endoscope and Standard Videoendoscope," Gastrointest. Endosc., **75**(2), pp. 373–381.
[27] Kummer, M. P., Abbott, J. J., Kratochvil, B. E., Borer, R., Sengul, A., and Nelson, B. J., 2010, "OctoMag: An Electromagnetic Systems for 5-DOF Wireless Micromanipulation," IEEE Trans. Robotics, **26**(6), pp. 1006–1017.
[28] Ciuti, G., Valdastri, P., Menciassi, A., and Dario, P., 2010, "Robotic Magnetic Steering and Locomotion of Capsule Endoscope for Diagnostic and Surgical Endoluminal Procedures," Robotica, **28**, pp. 199–207.
[29] "Matesy 3D-Magma," 2013, Matesy GmbH, Jena, Germany, http://www.3d-magma.de/